Superlattices and Microstructures 148 (2020) 106733

Contents lists available at ScienceDirect

Superlattices and Microstructures

journal homepage: www.elsevier.com/locate/superlattices

Role of threading dislocations and point defects in the performance of GaN-based metal-semiconductor-metal ultraviolet photodetectors

Abhishek Chatterjee [a,b,*], Shailesh K. Khamari [a], R. Kumar [a], S. Porwal [a], A. Bose [c], T. K. Sharma [a,b,**]

[a] Semiconductor Materials Lab., Raja Ramanna Centre for Advanced Technology, Indore, 452013, India
[b] Homi Bhabha National Institute, Training School Complex, Anushakti Nagar, Mumbai, 400094, India
[c] SCRF Cavity Characterization and Cryogenics Section, Raja Ramanna Centre for Advanced Technology, Indore, 452013, India

ARTICLE INFO

Keywords:
Threading dislocation
Point defects
Photoresponse
Schottky diode
GaN

ABSTRACT

The role of threading dislocations and point defects is investigated by comparing the performance of metal-semiconductor-metal ultraviolet photodetectors (PDs) fabricated on GaN epilayers grown by hydride vapour phase epitaxy (HVPE) and metal organic vapour phase epitaxy (MOVPE) techniques. It is found that the density of threading dislocations is higher in HVPE GaN epilayers, however, the devices fabricated on them show a higher photo response, lower leakage current and faster transient response when compared to those fabricated on MOVPE GaN epilayers. It is noticed that a high density of threading dislocations of HVPE grown GaN epilayers doesn't always restrict their usefulness in the development of specific devices. On the other hand, an inferior performance of PDs fabricated on MOVPE GaN epilayers is observed despite their low dislocation density, which is explained by considering the presence of point defects. Further, the room temperature electronic transport is found to be dominated by thermionic emission (thermionic field emission) mechanism in devices fabricated on GaN epilayers grown by HVPE (MOVPE) technique. In case of HVPE based devices, a switching of dominant transport mechanism is seen at ~200 K during cooling down whereas no such behaviour is observed for MOVPE based devices. Key factors affecting the performance of ultraviolet PDs fabricated on GaN epilayers grown by the two techniques and associated charge transport mechanisms are discussed.

1. Introduction

III-nitride based optoelectronic devices such as photodetectors (PDs) and light emitters are becoming increasingly popular due to their wide range of applications in strategic sectors, medical science, astronomy and commercial domain [1–4]. Due to their solar blind nature, radiation-resistance and thermal stability, these devices offer several advantages over conventional photomultiplier tubes and Si-based ultraviolet (UV) detectors, for example less operational complexities including the elimination of various filters [5–7]. Several types of GaN-based PDs, such as p-i-n diode [8], Schottky barrier [9], p–n junction [10] and metal–semiconductor–metal (MSM) [11]

* Corresponding author. Semiconductor Materials Lab., Raja Ramanna Centre for Advanced Technology, Indore, 452013, India.
** Corresponding author. Semiconductor Materials Lab., Raja Ramanna Centre for Advanced Technology, Indore, 452013, India.
E-mail addresses: cabhishek@rrcat.gov.in (A. Chatterjee), tarun@rrcat.gov.in (T.K. Sharma).

https://doi.org/10.1016/j.spmi.2020.106733
Received 2 May 2020; Received in revised form 4 August 2020; Accepted 21 October 2020
Available online 3 November 2020

PDs, have been reported during the past few years. Among them, MSM PDs are generally preferred due to their fabrication simplicity and easy integration with the field-effect-transistor based technology [12]. Although a remarkable progress has been made in the GaN material growth and device fabrication technology, there are several issues inherent to nitride based PDs which needs further investigations. For example, high-performance PDs demand a low dark current across the device since it sets a limit on the smallest measurable signal for a photodetector [13]. However, the mechanisms responsible for the generation of leakage current in GaN based UV PDs are still under debate. Extensive work is currently being carried out for identifying the origin of leakage current in GaN, where several possible sources like surface and interface traps [14–16], point defects [17–19] and threading dislocations are proposed to be the major contenders [20–22]. Among them, threading dislocations that are usually present in GaN epitaxial layers in large density, due to large lattice and thermal mismatch between GaN epi-layer and foreign substrate like sapphire, SiC, or Si, are assumed to be the primary source of leakage current in GaN. Recently, we also reported that the dislocations in GaN epilayers considerably influence the electronic conduction at all temperatures [23]. Other researchers have also reported that screw dislocations cause a sharp increase in the dark current of GaN UV PDs [24]. From scanning capacitance microscopy, Lucolano et al. [25] had shown that the core of threading dislocations behave as highly n-type doped regions. Due to this, a local lowering of Schottky barrier height takes place in those regions which triggers the onset of thermionic field emission (TFE) of carriers across the junction leading to a considerable increase in leakage current. Significant efforts have been made by many researchers for reducing the density of threading dislocations by incorporating low temperature grown buffer layers [26,27]. Involvement of SiN_x interlayer [28], substrate patterning, and innovative surface treatments of substrate have also been tried to improve the crystalline quality of GaN epitaxial layers. Irrespective of the progress reported via such attempts and the corresponding development of novel nitride devices, GaN epitaxial layers still possess a large density of threading dislocations. Moreover, several kinds of point defects such as N and/or Ga vacancies, interstitial and substitutional defects are also present in GaN, which along with threading dislocations are understood to make a substantial contribution to the leakage current [17,19]. Another key figure-of-merit of GaN PDs is their response to UV radiation. However, it is already known that threading dislocations considerably increase the recombination probability of photo-generated electron-hole pairs which leads to a significant reduction of the responsivity of GaN-based UV PDs [19]. Similar to their adverse effect on the leakage current, point defects are also known to reduce the photocurrent of GaN PDs by capturing the photo generated carriers [19]. Threading dislocations and point defects are expected to play a critical role in determining the overall performance of GaN UV PDs where a low density is generally preferred.

In this article, an in-depth characterization of GaN UV PDs is carried out with an aim of understanding the role of threading dislocations and point defects in device performance. It is found that a low density of threading dislocations in GaN epilayer doesn't necessarily ensure that the performance of the devices grown on top of it will always be superior. Key factors affecting the performance of UV PDs and associated charge transport mechanisms are also discussed by comparing the characteristics of devices fabricated on GaN epilayers grown by hydride vapour phase epitaxy (HVPE) and metal organic vapour phase epitaxy (MOVPE) techniques.

GaN/Sapphire templates grown by HVPE and MOVPE are commercially available and can be used to develop GaN based devices. Irrespective of a similar carrier concentration/type, electronic transport properties of the two templates are found to be very different [23]. In our earlier work [23], we had reported that the electronic transport was drastically affected by the charged dislocations formed at the layer-substrate interface in case of HVPE grown GaN epilayers whereas no such phenomenon was observed for MOVPE grown GaN. Suitable recommendations for choosing an appropriate GaN template for epitaxial growers were also made [23], where we had

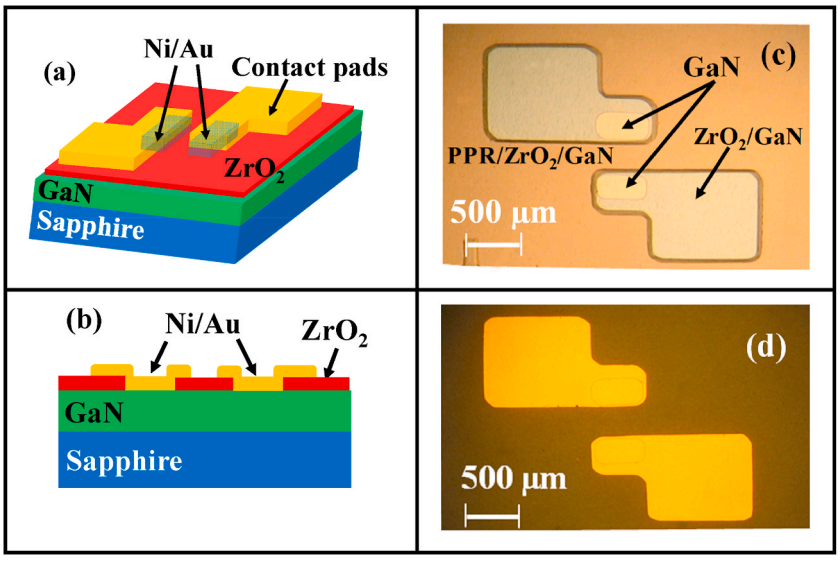

Fig. 1. (a) Schematic diagram showing the device structure, (b) cross-sectional view of the device, (c) optical microscopic image of the device after second step of photolithography prior to metallization where PPR stands for the positive photoresist, and (d) final device subsequent to the metallization and lift-off procedure.

concluded that "*HVPE grown templates are though cheaper than the MOVPE grown ones but these might limit the performance of a device grown on top of them*". However, we now find that MSM photodetectors fabricated on HVPE GaN epilayers show better device characteristics when compared to those fabricated on MOVPE GaN epilayers. Fundamental reasons behind the same are discussed in this article.

2. Experimental details

GaN epitaxial layers of 5 μm thickness grown on the c-plane Sapphire substrates are obtained from commercial vendors where samples A (B) are grown by using HVPE (MOVPE) technique respectively. Both the sample possess a room temperature carrier concentration of 2×10^{18} cm^{-3} which is estimated from Hall measurements [23]. Crystalline quality of the two samples is compared by performing ω-scans using High Resolution Panalytical X'Pert X-Ray Diffractometer (HRXRD) measurements with Cu $K\alpha_1$ X-rays ($\lambda = 1.54056$ Å). The samples are obtained by cutting the GaN templates into square pieces of 5×5 mm^2 size. Proper organic cleaning of the samples is carried out by boiling in trichloroethylene, acetone, methanol and then rinsing thoroughly in de-ionized water. Finally, a dilute HCl ($HCl:H_2O = 1:1$) treatment of samples is carried out for 10 s prior to the contact fabrication. Ohmic contacts are formed with Indium metal through rapid thermal annealing at 375 °C for 40 s in nitrogen ambient. Hall measurements on both the samples are performed under van der Pauw geometry [29,30]. Detail measurement procedure and electron transport properties of the two samples are discussed elsewhere [23,30]. In this work, GaN MSM UV PDs are fabricated by the two step mask-less photolithography [31]. A schematic diagram showing the device geometry is given in Fig. 1 (a) along with a cross-sectional view in Fig. 1 (b). Here, in the first step, a ZrO_2 oxide layer of 80 nm thickness is deposited by electron-beam evaporation under a base pressure of 5×10^{-6} mbar. The oxide layer is then patterned by photolithography and selectively etched by buffer HF solution for fabricating fingers of 500 μm length and 250 μm width along with a separation of 300 μm as shown in Fig. 1 (c). In second step, realignment and patterning is performed again for metallization and lift-off to obtain the final device with Ni/Au metal contact connecting the active device area with the large area contact pads on oxide layer as shown in Fig. 1(d). The oxide layer serves for the purpose of contact isolation and surface passivation. Temperature dependent I–V characteristics of the fabricated PDs are measured in dark and under illumination with a 325 nm UV laser and a Keithley 2450 source meter. Further, the room temperature spectral response of the device is measured using a 100 W Xenon lamp (excitation source), a 320 mm focal length monochromator, and a lock-in amplifier.

3. Results and discussion

It is necessary to evaluate the crystalline properties of the two GaN samples before we proceed to present the photoresponse of MSM devices. The density of dislocations in epitaxial layers can be estimated by HRXRD technique, which is usually preferred since one can access the layer quality rather quickly by simply comparing the full width at half maxima (FWHM) of corresponding diffraction peaks of respective samples. All types of dislocations are supposed to broaden the diffraction peaks and a low value of FWHM of HRXRD pattern is considered to be an evidence of good crystalline quality. FWHM of HRXRD patterns for (002) and (102) reflections of the two samples are listed in Table 1, where a low value is recorded for sample B. The values of tilt and twist are obtained from Williamson Hall analysis of ω-scans of symmetric (0 0 *l*) and skew symmetric (where either *h* or $k \neq 0$) set of (*h k l*) reflections and the corresponding values of dislocation density (N_D) are obtained by using the following relation [32–34]:

$$N_D = \frac{\beta^2}{4.35\ b^2} \tag{1}$$

where β is the tilt (twist) value for screw (edge) dislocations and b is the Burgers vector length ($b_{screw} = 0.5185$ nm, $b_{edge} = 0.3189$ nm). The density of screw and edge dislocations in the two GaN samples estimated from the Williamson Hall analysis is also shown in Table 1. It is found that the density of screw and edge dislocations is slightly higher for sample A, which confirms that the crystalline quality of sample B is better.

Fig. 2 shows the photoresponse of MSM PDs fabricated on both the samples over the spectral range of 300–390 nm at an applied bias of 4 V. It is surprising to see that the peak spectral response is enhanced by ~3 times for sample A in comparison to sample B. It is well-known that the edge dislocation lines provide acceptor traps and form negatively charged scattering centres in n-GaN [35]. It is reasonable to believe that the recombination probability of photo generated electron-hole pairs can be enhanced by the dislocation-induced acceptor levels which leads to a reduction in the responsivity of GaN PDs. Therefore, it is obvious to expect that the responsivity of GaN-based photodetectors made on sample A would be lower. Contrary to this, a high value of responsivity is recorded for this sample as obvious from Fig. 2. It seems plausible that the factors other than the dislocation density might determine the magnitude of photo-response in these devices.

Table 1
Microcrystalline properties of the two samples estimated from HRXRD measurements.

Sample	FWHM (arcsec)		Tilt (Degrees)	Twist (Degrees)	Screw dislocation density (N_{SD}) in cm^{-2}	Edge dislocation density (N_{ED}) in cm^{-2}
	(002)	(102)				
A	346	700	0.08	0.25	1.65×10^8	4.3×10^9
B	252	363	0.06	0.13	8.76×10^7	1.16×10^9

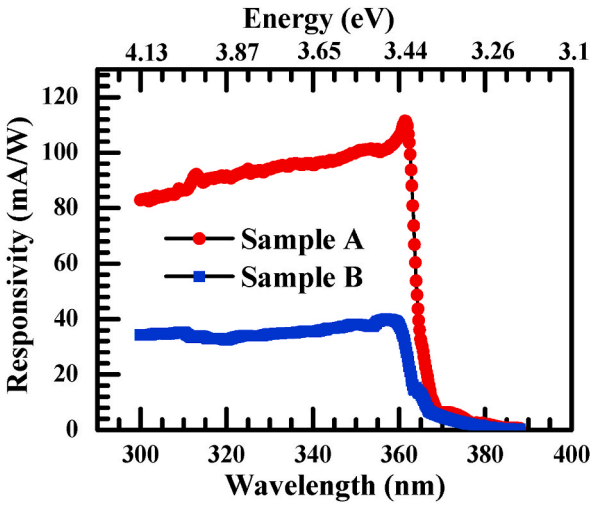

Fig. 2. Room temperature spectral response of GaN MSM Photodetectors.

In order to gain more information, transient response of the two devices is recorded as shown in Fig. 3. A fast transient response of PDs made on sample A is observed where rise (fall) times of 62 ms (375 ms) are measured in comparison to 1.06 s (1.40 s) for sample B. It therefore confirms that the devices made on sample A are superior. Further, the values of rise/fall time are highly acceptable, and similar values are recently reported by several researchers for GaN MSM PDs [36,37]. Note that relatively small dimensions are sometime preferred by researchers for the fabrication of GaN MSM devices [38], which generally helps in achieving a faster response. By keeping this in mind, a set of devices are fabricated where separation between the two contacts is reduced down to 150 μm. Transient response of such devices is found to be quite fast (μs time scale) which is actually governed by the instrumental limitation in our case. Although, small size of devices is sometime preferred but it might not provide a better representation of the sample quality in view of possible lateral variations in the density of dislocations and point defects. Since our aim here is to study the impact of the density of dislocations and point defects on the device performance, it is advisable to keep a large separation between the two contacts. In view of this, separation between the two contacts is varied over a rage of 300–1000 μm and the results from those devices are summarized in Fig. 4. It is interesting to see that though there is slight degradation of the responsivity with separation, which might be due to the inclusion of a larger number of dislocations and point defects, but an overall contrast in the responsivity of the two sets of devices remains intact. It therefore confirms that the photo response of HVPE based PDs (sample A) is few times larger than that of the MOVPE based devices (sample B), irrespective of the device size.

It is important to know if the observations made so far are consistent as a function of applied bias and excitation power. The outcome of such an exercise is shown in Fig. 5. The responsivity increases linearly with applied bias up to 2.5 V and tends to saturates thereafter as shown in Fig. 5(a). Such a behaviour of GaN photodetectors in already known [39,40]. Further, the photocurrent increases linearly with optical power at a constant bias under low excitation conditions, which leads to a constant value of responsivity as shown in Fig. 5(b).

Similar trends are already reported by other researchers under low power excitation conditions [41]. It is obvious that sample A has a larger responsivity irrespective of the value of applied bias or optical power. Moreover, the ratio of responsivity of two samples

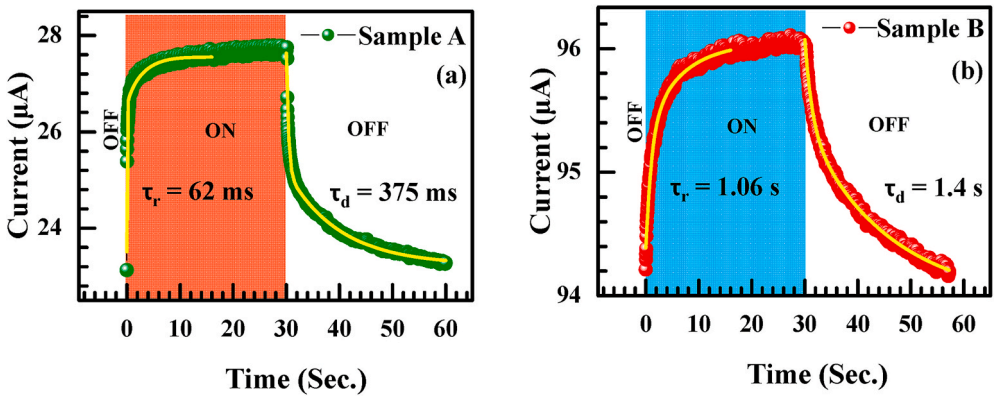

Fig. 3. Transient photoresponse of GaN MSM Photodetectors made on a) Sample A, and b) Sample B, where yellow solid lines represent an exponential fit of corresponding part of the experimental data.

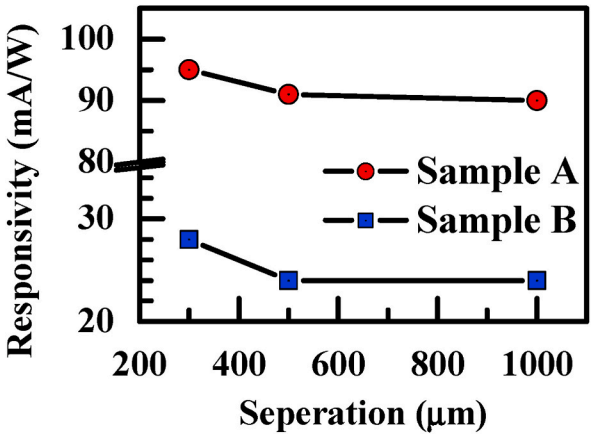

Fig. 4. Responsivity of GaN MSM Photodetectors plotted as a function of separation between the two contacts, error bars in the data are smaller than the size of symbols.

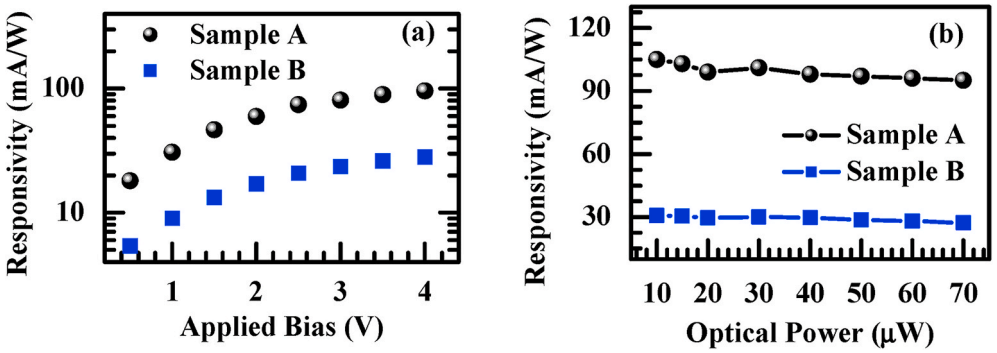

Fig. 5. Responsivity of GaN MSM Photodetectors as a function of (a) applied bias at 50 μW, and (b) optical power at 4 V for sample A and B.

remains more or less constant. It is therefore obvious that the photodetectors made on sample A demonstrate better device characteristics under all the operating conditions. It indicates that the factors other than the dislocation density play a critical role in governing the performance of GaN MSM PDs.

In order to pinpoint the fundamental reasons behind the high performance of PDs made on HVPE GaN epilayers, detailed electronic

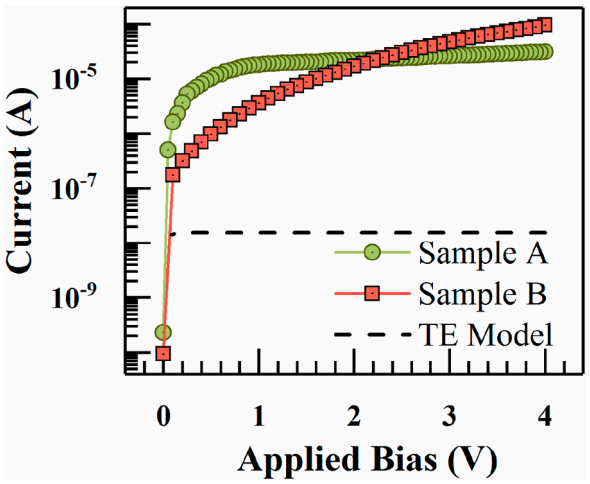

Fig. 6. Room temperature I-V characteristics of the two GaN samples. Theoretical curve based on the Thermionic emission (TE) model is also shown for comparison purpose.

transport measurements are performed on the two samples. It is generally understood that a low screw dislocation density will lead to a lower dark current in PDs [22]. As can be seen from Fig. 6, it is indeed true in case the applied bias is kept below 2 V where dark current of sample A is higher than that of sample B. However, the situation is just opposite if the applied bias is kept above 2 V. It is surprising to note that the dark current of PDs made out of sample A, which possesses relatively high dislocation density, is lower than that of sample B under high bias condition. Moreover, slope of the two curves is also seen to be very different. Further, it is sample B which shows a much larger difference from the theoretically estimated curve based on the thermionic emission (TE) transport model [21] compared to sample A. It is noticed that the leakage current shows a much stronger dependence on applied bias in sample B.

In case of III-nitrides, it is well known that the threading dislocations and point defects provide an alternate path for charge conduction, which often lead to a considerably large leakage current [19,21,42]. Thus, the thermionic field emission (TFE) process mediated by carrier tunnelling can be considered as a probable mechanism which can explain the I–V characteristics shown in Fig. 6. TFE model as proposed by Padovani and Stratton [43] is based on the Taylor expansion of tunnelling probability under WKB approximation and can be expressed as

$$I_{TFE} = I_{TFE,S} \exp\left(\frac{qV_R}{\zeta}\right) \tag{2}$$

where $I_{TFE,S}$ is the saturation current, V_R is the applied bias, and parameter ζ is expressed as $\zeta = E_{00}\left[\left(\frac{E_{00}}{kT}\right) - \tanh\left(\frac{E_{00}}{kT}\right)\right]^{-1}$ where k is the Boltzmann constant, T is the temperature in Kelvin and E_{00} is the characteristic tunnelling energy given by $E_{00} = \frac{\hbar q}{2}\sqrt{\frac{N_d}{\varepsilon_s \varepsilon_0 m_e^*}}$. Here, N_d is the doping density, ε_s is the dielectric constant of GaN, ε_o is the permittivity of free space and m_e^* is effective mass of electron. Note that a large value of E_{00} indicates about the dominance of TFE mechanism in charge transport [21]. It is observed that I–V characteristics of both the samples can be reasonably fitted by Eqn. (2) over a wide temperature range, as shown in Fig. 7. This presents a direct evidence of the dominance of TFE mechanism in our case. The values of E_{00} obtained from the fitting procedure are plotted in Fig. 8 for both the samples. A considerably high value of E_{00} in both the samples at low temperature indicates that TFE is the dominant current transport mechanism in this temperature regime. Such an observation is already reported by us in HVPE grown GaN samples where the presence of a large density of dislocations at the GaN/sapphire interface is found to be responsible for this behaviour [7,21,23,44]. Further, a downward trend in the values of E_{00} can be observed with increasing temperature in both the samples.

Note that E_{00} reduces from 7.6 (8.2) to 2.9 (6.0) meV with rise of temperature from 10 to 300 K for sample A (B) respectively. Moreover, an abrupt change is observed in sample A at ~200 K. On the other hand, slope of the curve is not that steep in sample B. These observations indicate that the carrier transport mechanism changes in sample A at ~200 K.

In order to gain further understanding of the impact of carrier tunnelling on the dark current, Schottky barrier height of the two samples are plotted as a function of temperature in Fig. 9. For this purpose, Ni/Au Schottky contacts are fabricated on one side of the sample while Indium is used to make Ohmic contact on the other side. The values of Schottky barrier height shown in Fig. 9 are determined from the forward bias I-V curve considering TE model [21]. It is found that the barrier height monotonically increases with temperature for both the samples. Such a trend is very common in GaN samples where interfacial defects and dislocation-related current paths are reported to be responsible for such non-ideal behaviour of Schottky contact [21,45]. This can be very well explained by considering the TFE mechanisms of carrier across the regions surrounding the core of dislocations as discussed earlier [21]. An interesting observation can be made from Fig. 9 where the barrier height for sample A is seen to be larger than that of sample B at all temperatures. It is really surprising since the screw component of threading dislocations, which is responsible for lowering the barrier height in GaN [21,22], is measured to be rather high in sample A as shown in Table 1. It therefore indicates that factors other than the dislocations seems to play a more decisive role in lowering (raising) the barrier height (leakage current) in sample B respectively and the same argument can also be applied to understand the contrast observed in the responsivity and transient response of the two samples. As discussed earlier that many kinds of point defects are present in GaN [17] and it is highly possible that those

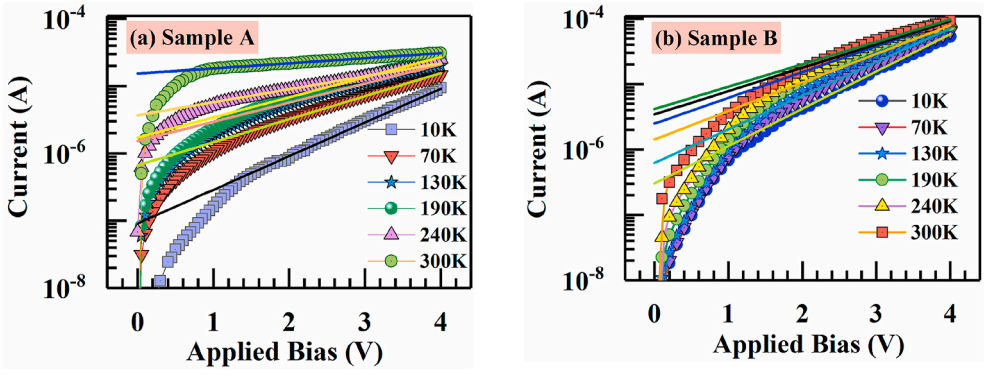

Fig. 7. Temperature dependent I-V characteristics of (a) sample A, and (b) sample B where the respective solid lines show the corresponding theoretical curves based on the TFE model.

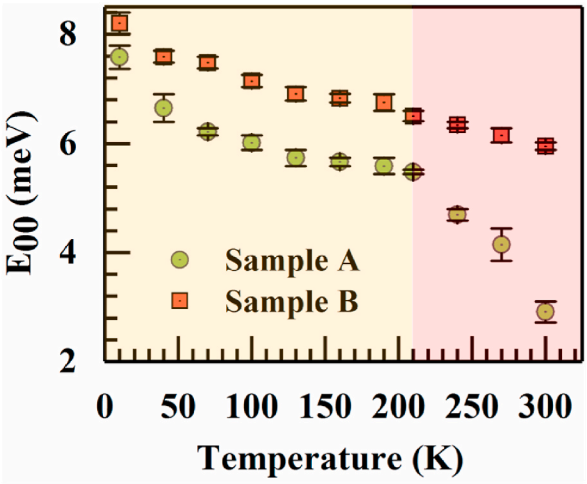

Fig. 8. Temperature dependence of characteristic tunnelling energy (E_{00}) shown for the two GaN samples, error bars includes both the statistical and fitting errors. Regions showing a steep change in E_{00} values for sample A are highlighted by shading with different colours.

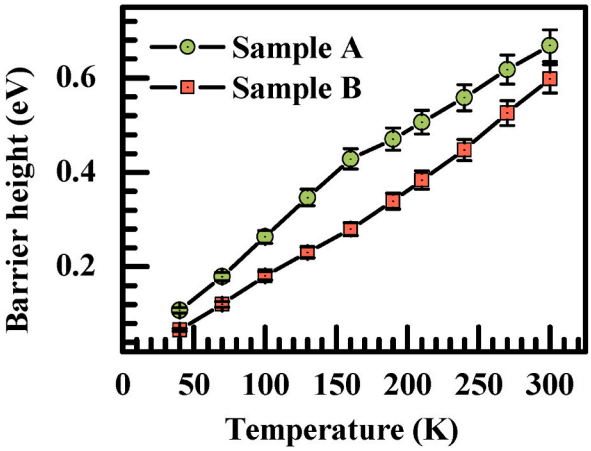

Fig. 9. Schottky barrier height versus temperature for the two GaN samples. The data points are shown with error bars that includes both the statistical and instrumental errors.

might be responsible for the fall (rise) of barrier height (leakage current), and also a low value of responsivity in sample B irrespective of its low dislocation density. It is already known that n-type GaN layers grown by MOVPE are intentionally doped with Silicon and the same is also confirmed by the vendor. Hall and C-V data are in good agreement for sample B as reported earlier [23], a complete ionization of donor atoms is thus expected. Hence, Si doping level is estimated to be of the order of $\sim 2 \times 10^{18}$ cm^{-3} for sample B. Such a high intentional doping leads to an increase in the leakage current in this sample. From positron annihilation measurements, Zhao et al. [19] reported that even light doping with Si can increase the concentration of Ga vacancies in n-type GaN in comparison to undoped samples. Such Ga vacancies act as deep level defects leading to further rise of leakage current in sample B.

On the other hand, Si doping level of HVPE GaN epilayers is $\sim 1 \times 10^{16}$ cm^{-3} only as estimated from the secondary ion mass spectrometry (SIMS) profile provided by the vendor, which indicates about a low density of point defects in the depletion region of sample A. The sources of doping in HVPE grown GaN epilayers turns out to be very different where a dominant contribution to carrier concentration occurs due to oxygen impurities that cluster around dislocation sites leading to the formation of a highly doped impurity channel [23,46]. It provides a low resistive path for the electronic transport, which apparently increase the background carrier density of sample A. Similar differences in the doping behaviour of the two samples are also observed by us in SIMS measurements. However, the carrier concentration at the edge of the depletion width of Schottky junction obtained from the capacitance-voltage (C-V) analysis is found to be two order less in sample A as reported by us earlier [23]. Further, the values of carrier concentration estimated from C-V measurements are more relevant in case of MSM PDs due to the formation of Schottky junction. Hence, it can be concluded that the photodetectors fabricated on sample A with undoped GaN provide a much lower leakage current, even though those are having a higher dislocation density. With this model, the observed temperature dependence of E_{00} and barrier height of the two samples can now be explained very well. It is already reported that the areal contribution of highly n-type regions surrounding dislocation cores is

only 2–3% of entire Schottky area [25]. Therefore, their contribution is limited at high temperatures where TE mechanism associated with the large junction area plays a major role in the carrier transport. This mechanism leads to a dramatic reduction in the value of E_{00} in sample A in the high temperature range i.e. above ~200 K. Moreover, the dominant transport mechanism switches from TE to TFE during the cooling down process at ~200 K. On the other hand, TFE is the primary transport mechanism in the intentionally doped sample B at all temperatures leading to a comparatively weak temperature dependence of E_{00}. Temperature dependence of barrier height can also be explained on similar lines where sample A always maintains a high barrier since the screw dislocations responsible for the TFE transport are activated within a very small region of the total area. On the other hand, in sample B, entire junction area takes part in the carrier transport.

Next, the same argument can also be used to explain the contrast observed in the performance of two sets of devices shown in Figs. 2 and 3. Since the drift component dominates the photocurrent in our devices, the magnitude of photo-response will be significantly influenced by the density of photo generated carriers that are available in the depletion region. The zero bias depletion width estimated from C-V measurements for sample A and B are 425 and 30 nm respectively [23]. It is numerically calculated that the photo response will be enhanced by a factor of ~4 in sample A due to the enlarged depletion width. It can partially explain the observed difference in the responsivity of two samples plotted in Fig. 2. Note that the density of screw and edge dislocations is few times higher for sample A which reduces the contrast in the responsivity of two samples. Had it not been the case then the measured difference between the photoresponse of two devices would have been larger. Another point which needs to be explained is the faster response of devices as shown in Fig. 3. It can be understood by considering the role of point defects in sample B as mentioned earlier. It is already known that Si doping increases the concentration of Ga vacancies which reduces the minority carrier diffusion length due to the presence of deep level defects [19]. Ga vacancies trap the photo generated carriers in depletion region leading to the observed reduction in the speed of PDs fabricated on sample B [47,48]. Further, absorption of excitation beam beyond the depletion width in sample B brings the diffusion component into play, which provides another reason for a slow response of the devices. It is also noticed that the exciton feature is clearly visible in terms of a sharp peak at 361 nm in the spectral response of sample A shown in Fig. 2, which is considerably supressed in sample B. Absence of excitonic feature can be explained by considering a high density of free carriers in sample B which screens the Coulomb interaction and reduces the exciton binding energy [49]. It also explains why a flat spectral response is observed in the above band gap region of sample B whereas a rise in the responsivity is seen with wavelength for sample A in Fig. 2. At shorter wavelength, an enhanced absorption of incident photons near the surface causes a fall in the responsivity due to the capture of photo excited carriers by the surface states. A flat spectral response of PDs made on HVPE GaN layers is already demonstrated by us after a proper surface passivation via deposition of thin ZrO_2 layer [44]. A high density of ionized donors near the sample surface leads to a narrow depletion width in sample B and also minimizes the impact of surface states on the spectral response at shorter wavelength as shown in Fig. 2.

4. Conclusion

Metal-semiconductor-metal ultraviolet photodetectors are fabricated on n-GaN epitaxial layers grown by HVPE and MOVPE techniques. Contrary to the general understanding, the photo response of HVPE based PDs is found to be ~3 times larger than that of the MOVPE based devices. Further, the overall performance of HVPE based PDs turns out to be better than that those fabricated on MOVPE GaN, in spite of the variations in device geometry or the operating conditions. It is explained by considering the difference in the depletion width which is primarily governed by the different procedures adopted for the doping of GaN templates. A large carrier concentration at the edge of depletion width in MOVPE grown GaN epilayer leads to higher (lower) leakage current (barrier height) despite a low dislocation density. In temperature dependent I-V measurements, a sharp change in the value of characteristics tunnelling energy is seen at ~200 K for HVPE based devices whereas no such behaviour is seen for PDs fabricated on MOVPE grown epilayers. This is explained by considering the switching of electronic transport mechanism from TE to TFE during the cooling down. On the other hand, TFE is found to be the dominant transport mechanism in devices fabricated on MOVPE grown epilayers. It is hereby concluded that controlling the density of threading dislocations is not the sole criteria for improving the performance of GaN Schottky PDs, rather one also need to be careful about the density of point defects which can also marginalize the key figure-of-merits. The understanding developed here is expected to be helpful in making a judicious choice of GaN templates for the development of specific devices based on them.

Author statement

Abhishek Chatterjee: Conceptualization, Methodology, Investigation, Writing- Original draft preparation; Shailesh K. Khamari: Writing- Reviewing and Editing; R. Kumar: HRXRD data Analysis; S. Porwal: Optical Spectroscopy; A. Bose: SIMS measurement; T. K. Sharma: Supervision.

Declaration of competing interest

The authors declare that they have no known competing financial interests or personal relationships that could have appeared to influence the work reported in this paper.

Acknowledgement

Authors acknowledge Dr. V. K. Dixit for many useful discussions, Mr. Subhomay Haldar for mask less lithography system, Dr. Neha Sharma for AFM measurements, Mr. U. K. Ghosh, Mr. Alexander Khakha, Mr. Vishal Agnihotri and Mr. A. K. Jaiswal for the technical support.

References

[1] S.J. Pearton, J.C. Zolper, R.J. Shul, F. Ren, J. Appl. Phys. 86 (1999) 1.
[2] M.J. Eccles, M.E. Sim, K.P. Tritton, Low Light Level Detectors in Astronomy, Cambridge University Press, Cambridge, England, 1983.
[3] J.L. Pau, C. Rivera, J. Pereiro, E. Muñoz, E. Calleja, U. Schühle, E. Frayssinet, B. Beaumont, J.P. Faurie, Superlattice. Microst. 36 (2004) 807–814.
[4] P. Gibartc, M. Razeghi, A. Rogalsky, J. Appl. Phys. 79 (1996) 7433.
[5] M. Khan, M. Shatalov, H. Maruska, H. Wang, E. Kuokstis, Jpn. J. Appl. Phys., Part 1 (44) (2005) 7191.
[6] M. Brendel, M. Helbling, A. Knigge, F. Brunner, M. Weyers, J. Appl. Phys. 118 (2015) 244504.
[7] A. Chatterjee, S.K. Khamari, S. Porwal, S. Kher, T.K. Sharma, J. Appl. Phys. 123 (2018) 161585.
[8] Y. Kang, Y. Xu, D. Zhao, J. Fang, Solid State Electron. 49 (2005) 1135–1139.
[9] Q.N. Abdullah, A.R. Ahmed, A.M. Ali, F.K. Yam, Z. Hassan, M. Bououdina, M.A. Almessiere, Superlattice. Microst. 117 (2018) 92–104.
[10] M.Z. Mohd Yusoff, A. Baharin, Z. Hassan, H. Abu Hassan, M.J. Abdullah, Superlattice. Microst. 56 (2013) 35–44.
[11] N. Zainal, M.A. Ahmad, W. Maryam, M.E.A. Samsudin, S.N. Waheeda, M. Ikram Md. Taib, Z. Hassan, Superlattice. Microst. 138 (2020) 106369.
[12] T. Palacios, E. Monroy, F. Calle, F. Omnes, Appl. Phys. Lett. 81 (2002) 1902.
[13] F. Xie, H. Lu, X. Xiu, D. Chen, P. Han, R. Zhang, Y. Zheng, Solid State Electron. 57 (2011) 39.
[14] Y.H. Chen, K. Zhang, M.Y. Cao, S.L. Zhao, J.C. Zhang, X.H. Ma, Y. Hao, Appl. Phys. Lett. 104 (2014) 153509.
[15] C. Lu, X. Zhang, X. Xie, S. Feng, I. Diagne, A. Khan, S.N. Mohammad, J. Vac. Sci. Technol., B 26 (2008) 1987.
[16] H. Hasegawa, S. Oyama, J. Vac. Sci. Technol., B 20 (2002) 1647.
[17] M.A. Reshchikov, H.J. Morkoc, Appl. Phys. 97 (2005), 061301.
[18] F.S. Choi, J.T. Griffiths, Chris Ren, K.B. Lee, Z.H. Zaidi, P.A. Houston, I. Guiney, C.J. Humphreys, R.A. Oliver, D.J. Wallis, J. Appl. Phys. 124 (2018), 055702.
[19] D.G. Zhao, D.S. Jiang, J.J. Zhu, Z.S. Liu, S.M. Zhang, J.W. Liang, Hui Yang, X. Li, X.Y. Li, H.M. Gong, Appl. Phys. Lett. 90 (2007), 062106.
[20] E.J. Miller, D.M. Schaadt, E.T. Yu, X.L. Sun, L.J. Brillson, P. Waltereit, J.S. Speck, J. Appl. Phys. 94 (2003) 7611.
[21] A. Chatterjee, S.K. Khamari, V.K. Dixit, S.M. Oak, T.K. Sharma, J. Appl. Phys. 118 (2015) 175703.
[22] D. Li, X. Sun, H. Song, Z. Li, Y. Chen, G. Miao, H. Jiang, Appl. Phys. Lett. 98 (2011), 011108.
[23] A. Chatterjee, S.K. Khamari, R. Kumar, V.K. Dixit, S.M. Oak, T.K. Sharma, Appl. Phys. Lett. 106 (2015), 023509.
[24] E.J. Miller, D.M. Schaadt, E.T. Yu, C. Poblenz, C. Elsass, J.S. Speck, J. Appl. Phys. 91 (2002) 9821.
[25] F. Iucolano, F. Roccaforte, F. Giannazzo, V. Raineri J, Appl. Phys. 102 (2007) 113701.
[26] M.A. Morama, M.J. Kappers, T.B. Joyce, P.R. Chalker, Z.H. Barber, C.J. Humphreys, J. Cryst. Growth 308 (2007) 302.
[27] P.V. Parphenyuk, A.A. Evtukh, Semiconductor physics, Quant. Electron. Optoelectron. 19 (2016) 1.
[28] Zhen Huang, Yuantao Zhang, Gaoqiang Deng, Baozhu Li, Shuang Cui, Hongwei Liang, Yuchun Chang, Junfeng Song, Baolin Zhang, Guotong Du, J. Mater. Sci.: Mater. Electron. 27 (2016) 10003.
[29] D.C. Look, Electrical Characterization of GaAs Materials and Devices, first ed., John Wiley & Sons, New York, 1989.
[30] A. Chatterjee, S.K. Khamari, V.K. Dixit, T.K. Sharma, S.M. Oak, Physics of Semiconductor Devices, Environmental Science and Engineering, Springer, 2014, p. 767.
[31] S. Haldar, G. Vashisht, U.K. Ghosh, A.K. Jaiswal, S. Porwal, A. Khakha, T.K. Sharma, V.K. Dixit, AIP Conf. Proc. 2115 (2019), 030219.
[32] M.A. Moram, M.E. Vickers, Rep. Prog. Phys. 72 (2009), 036502.
[33] H. Heinke, V. Kirchner, S. Einfeldt, D. Hommel, Appl. Phys. Lett. 77 (2000) 2145.
[34] R. Kumar, T. Ganguli, V. Chouhan, V.K. Dixit, J. Nano-Electron. Phys. 3 (2011) 17.
[35] N.G. Weimann, L.F. Eastman, D. Doppalapudi, H.M. Ng, T.D. Moustakas, J. Appl. Phys. 83 (1998) 3656.
[36] A. Gundimeda, S. Krishna, N. Aggarwal, A. Sharma, N.D. Sharma, K.K. Maurya, S. Husale, G. Gupta, Appl. Phys. Lett. 110 (2017) 103507.
[37] N. Prakash, M. Singh, G. Kumar, A. Barvat, K. Anand, P. Pal, S.P. Singh, S.P. Khanna, Appl. Phys. Lett. 109 (2016) 242102.
[38] D. Walker, E. Monroy, P. Kung, J. Wu, M. Hamilton, F.J. Sanchez, J. Diaz, M. Razeghi, Appl. Phys. Lett. 74 (1999) 762.
[39] K.S. Stevens, M. Kinniburgh, R. Beresford, Appl. Phys. Lett. 66 (1995) 3518.
[40] Bo Shen, Kai Yang, Zang Lan, Zhi-zhong Chen, Yu-gang Zhou, Peng Chen, Rong Zhang, Zheng-chun Huang, Hao-shen Zhou, You-dou Zheng, Jpn. J. Appl. Phys. 38 (1999) 767.
[41] F. Binet, J.Y. Duboz, E. Rosencher, F. Scholz, V. Härle, Appl. Phys. Lett. 69 (1996) 1202.
[42] B.S. Simpkins, E.T. Yu, P. Waltereit, J.S. Speck, J. Appl. Phys. 94 (2003) 1448.
[43] F.A. Padovani, R. Stratton, Solid State Electron. 9 (1966) 695.
[44] A. Chatterjee, S.K. Khamari, S. Porwal, T.K. Sharma, Phys. Stat. Solidi RRL 13 (2019) 1900265.
[45] L.S. Yu, Q.Z. Liu, Q.J. Xing, D.J. Qiao, S.S. Lau, J. Redwing, J. Appl. Phys. 84 (1998) 2099.
[46] T. Zhu, R.A. Oliver, Phys. Chem. Chem. Phys. 14 (2012) 9558–9573.
[47] J. Elsner, R. Jones, M.I. Heggie, P.K. Sitch, M.L. Haugk, Th. Frauenheim, S. Öberg, P.R. Griddon, Phys. Rev. B 58 (1998) 12571.
[48] C.B. Soh, S.J. Chua, H.F. Lim, D.Z. Chi, S. Tripathy, W. Liu, J. Appl. Phys. 96 (2004) 1341.
[49] M. Fox, Optical Properties of Solids, Oxford University Press, New York, 2001.